Research Article | Vol. 7, No. 10 | 1 Oct 2016 | BIOMEDICAL OPTICS EXPRESS 3958
Biomedical Optics EXPRESS

Scanless functional imaging of hippocampal networks using patterned two-photon illumination through GRIN lenses

CLAUDIO MORETTI,[1] ANDREA ANTONINI,[1,2] SERENA BOVETTI,[1] CARLO LIBERALE,[2,3] AND TOMMASO FELLIN[1,*]

[1]*Optical Approaches to Brain Function Laboratory, Department of Neuroscience and Brain Technologies, Istituto Italiano di Tecnologia, Via Morego 30, 16163 Genova, Italy*
[2]*Nanostructures Department, Istituto Italiano di Tecnologia, Via Morego 30, 16163 Genova, Italy*
[3]*BESE Division, King Abdullah University of Science and Technology (KAUST), Thuwal 23955-6900, Saudi Arabia*
[*]*tommaso.fellin@iit.it*

Abstract: Patterned illumination through the phase modulation of light is increasingly recognized as a powerful tool to investigate biological tissues in combination with two-photon excitation and light-sensitive molecules. However, to date two-photon patterned illumination has only been coupled to traditional microscope objectives, thus limiting the applicability of these methods to superficial biological structures. Here, we show that phase modulation can be used to efficiently project complex two-photon light patterns, including arrays of points and large shapes, in the focal plane of graded index (GRIN) lenses. Moreover, using this approach in combination with the genetically encoded calcium indicator GCaMP6, we validate our system performing scanless functional imaging in rodent hippocampal networks *in vivo* ~1.2 mm below the brain surface. Our results open the way to the application of patterned illumination approaches to deep regions of highly scattering biological tissues, such as the mammalian brain.

OCIS codes: (170.2150) Endoscopic imaging; (180.4315) Nonlinear microscopy; (120.5060) Phase modulation; (170.2520) Fluorescence microscopy.

References and links

1. T. Knöpfel, "Genetically encoded optical indicators for the analysis of neuronal circuits," Nat. Rev. Neurosci. **13**(10), 687–700 (2012).
2. F. Zhang, A. M. Aravanis, A. Adamantidis, L. de Lecea, and K. Deisseroth, "Circuit-breakers: optical technologies for probing neural signals and systems," Nat. Rev. Neurosci. **8**(8), 577–581 (2007).
3. F. Zhang, V. Gradinaru, A. R. Adamantidis, R. Durand, R. D. Airan, L. de Lecea, and K. Deisseroth, "Optogenetic interrogation of neural circuits: technology for probing mammalian brain structures," Nat. Protoc. **5**(3), 439–456 (2010).
4. V. Nikolenko, B. O. Watson, R. Araya, A. Woodruff, D. S. Peterka, and R. Yuste, "SLM Microscopy: Scanless Two-Photon Imaging and Photostimulation with Spatial Light Modulators," Front. Neural Circuits **2**, 5–19 (2008).
5. M. Dal Maschio, F. Difato, R. Beltramo, A. Blau, F. Benfenati, and T. Fellin, "Simultaneous two-photon imaging and photo-stimulation with structured light illumination," Opt. Express **18**(18), 18720–18731 (2010).
6. M. Dal Maschio, A. M. De Stasi, F. Benfenati, and T. Fellin, "Three-dimensional in vivo scanning microscopy with inertia-free focus control," Opt. Lett. **36**(17), 3503–3505 (2011).
7. S. Quirin, D. S. Peterka, and R. Yuste, "Instantaneous three-dimensional sensing using spatial light modulator illumination with extended depth of field imaging," Opt. Express **21**(13), 16007–16021 (2013).
8. S. Quirin, J. Jackson, D. S. Peterka, and R. Yuste, "Simultaneous imaging of neural activity in three dimensions," Front. Neural Circuits **8**, 29 (2014).
9. S. J. Yang, W. E. Allen, I. Kauvar, A. S. Andalman, N. P. Young, C. K. Kim, J. H. Marshel, G. Wetzstein, and K. Deisseroth, "Extended field-of-view and increased-signal 3D holographic illumination with time-division multiplexing," Opt. Express **23**(25), 32573–32581 (2015).
10. W. Yang, J. E. Miller, L. Carrillo-Reid, E. Pnevmatikakis, L. Paninski, R. Yuste, and D. S. Peterka, "Simultaneous Multi-plane Imaging of Neural Circuits," Neuron **89**(2), 269–284 (2016).
11. S. Bovetti and T. Fellin, "Optical dissection of brain circuits with patterned illumination through the phase modulation of light," J. Neurosci. Methods **241**, 66–77 (2015).

#269402 http://dx.doi.org/10.1364/BOE.7.003958
Journal © 2016 Received 1 Jul 2016; revised 25 Aug 2016; accepted 6 Sep 2016; published 12 Sep 2016

Biomedical Optics EXPRESS

12. E. Papagiakoumou, V. de Sars, D. Oron, and V. Emiliani, "Patterned two-photon illumination by spatiotemporal shaping of ultrashort pulses," Opt. Express **16**(26), 22039–22047 (2008).
13. E. Papagiakoumou, V. de Sars, V. Emiliani, and D. Oron, "Temporal focusing with spatially modulated excitation," Opt. Express **17**(7), 5391–5401 (2009).
14. E. Papagiakoumou, F. Anselmi, A. Bègue, V. de Sars, J. Glückstad, E. Y. Isacoff, and V. Emiliani, "Scanless two-photon excitation of channelrhodopsin-2," Nat. Methods **7**(10), 848–854 (2010).
15. E. Papagiakoumou, A. Bégue, B. Leshem, O. Schwartz, B. M. Stell, J. Bradley, D. Oron, and V. Emiliani, "Funtional patterned multiphoton excitation deep inside scattering tissue," Nat. Photonics **7**(4), 274–278 (2013).
16. A. Bègue, E. Papagiakoumou, B. Leshem, R. Conti, L. Enke, D. Oron, and V. Emiliani, "Two-photon excitation in scattering media by spatiotemporally shaped beams and their application in optogenetic stimulation," Biomed. Opt. Express **4**(12), 2869–2879 (2013).
17. A. M. Packer, L. E. Russell, H. W. Dalgleish, and M. Hausser, "Simultaneous all-optical manipulation and recording of neural circuit activity with cellular resolution in vivo," Nat. Methods **12**(2), 140–146 (2014).
18. J. P. Rickgauer, K. Deisseroth, and D. W. Tank, "Simultaneous cellular-resolution optical perturbation and imaging of place cell firing fields," Nat. Neurosci. **17**(12), 1816–1824 (2014).
19. K. König, M. Weinigel, D. Hoppert, R. Bückle, H. Schubert, M. J. Köhler, M. Kaatz, and P. Elsner, "Multiphoton tissue imaging using high-NA microendoscopes and flexible scan heads for clinical studies and small animal research," J. Biophotonics **1**(6), 506–513 (2008).
20. R. P. Barretto, B. Messerschmidt, and M. J. Schnitzer, "In vivo fluorescence imaging with high-resolution microlenses," Nat. Methods **6**(7), 511–512 (2009).
21. Grintech product datasheet, "High-NA Endomicroscopic Imaging Objective for 2-Photon Microscopy" (Grintech, 2016). *http://www.grintech.de/grin-lens-systems-for-medical-applications.html*
22. C. J. R. Sheppard and M. Gu, "Image formation in two-photon fluroescence microscopy," Optik (Stuttg.) **86**, 104–106 (1990).
23. F. Helmchen and W. Denk, "Deep tissue two-photon microscopy," Nat. Methods **2**(12), 932–940 (2005).
24. F. Anselmi, C. Ventalon, A. Bègue, D. Ogden, and V. Emiliani, "Three-dimensional imaging and photostimulation by remote-focusing and holographic light patterning," Proc. Natl. Acad. Sci. U.S.A. **108**(49), 19504–19509 (2011).
25. A. Antonini, C. Liberale, and T. Fellin, "Fluorescent layers for characterization of sectioning microscopy with coverslip-uncorrected and water immersion objectives," Opt. Express **22**(12), 14293–14304 (2014).
26. R. Di Leonardo, F. Ianni, and G. Ruocco, "Computer generation of optimal holograms for optical trap arrays," Opt. Express **15**(4), 1913–1922 (2007).
27. V. A. Soifer, *Methods for Computer Design of Diffractive Optical Elements*, (John Wiley & Sons, Inc., 2002).
28. D. Gandolfi, P. Pozzi, M. Tognolina, G. Chirico, J. Mapelli, and E. D'Angelo, "The spatiotemporal organization of cerebellar network activity resolved by two-photon imaging of multiple single neurons," Front. Cell. Neurosci. **8**, 92 (2014).
29. T. W. Chen, T. J. Wardill, Y. Sun, S. R. Pulver, S. L. Renninger, A. Baohan, E. R. Schreiter, R. A. Kerr, M. B. Orger, V. Jayaraman, L. L. Looger, K. Svoboda, and D. S. Kim, "Ultrasensitive fluorescent proteins for imaging neuronal activity," Nature **499**(7458), 295–300 (2013).
30. G. Paxinos and K. B. J. Franklin, *The Mouse Brain in Stereotaxic Coordinates* (Academic Press, ed., 2012).
31. M. E. Bocarsly, W. C. Jiang, C. Wang, J. T. Dudman, N. Ji, and Y. Aponte, "Minimally invasive microendoscopy system for in vivo functional imaging of deep nuclei in the mouse brain," Biomed. Opt. Express **6**(11), 4546–4556 (2015).
32. V. Szabo, C. Ventalon, V. De Sars, J. Bradley, and V. Emiliani, "Spatially selective holographic photoactivation and functional fluorescence imaging in freely behaving mice with a fiberscope," Neuron **84**(6), 1157–1169 (2014).

1. Introduction

The development of efficient light-dependent sensors [1] and actuators [2,3] is dramatically improving our understanding of brain function by enabling remote monitoring and control of the electrical activity in specific subsets of cells. In parallel, new optical approaches have been introduced to fully exploit the potential of these novel molecular tools. For example, patterned two-photon illumination through the phase modulation of light (from now on called patterned illumination) has been used to spatially and dynamically multiplex the laser beam to perform scanless imaging in combination with fluorescence activity reporters [4–10]. In scanless imaging simultaneous illumination of multiple areas of the sample is performed, allowing high-speed recording of functional signals at multiple locations [11]. Moreover, patterned illumination has been used to restrict two-photon light to extended shapes [12,13]. In combination with light-sensitive optogenetic probes, this has allowed cell-specific electrical activation of individual neurons [14–18]. However, since light is scattered by the brain tissue and all the aforementioned studies employed standard microscope objectives, the

Biomedical Optics EXPRESS

applicability of two-photon patterned illumination is currently limited to the more superficial regions of the mammalian brain. To deliver light to deeper structures, small optical probes, such as GRIN rods or GRIN microobjectives [19,20], must be used but patterned two-photon illumination through these GRIN probes has not been described before. Here, we developed an optical system based on phase modulation through a liquid crystal spatial light modulator (SLM) and demonstrated efficient patterned two-photon illumination with GRIN lenses-based endomicroscopes. Using this approach, we demonstrate efficient recording of GCaMP6 signals in the scanless configuration from hippocampal CA1 cells located ~1.2 mm deep within the mouse brain *in vivo*.

2. Experimental set-up

The main setup is shown in Fig. 1(a). It was based on a commercial two-photon laser scanhead (Bruker Corp., Billerica, MA, former Prairie Technologies, Madison, WI) and a customized holder for the GRIN rod or the GRIN microobjective which ensured proper coupling between the GRIN probe and the used objective for *in vitro* recordings (Fig. 1(b)). In imaging experiments *in vivo*, the GRIN lens was implanted into the brain tissue (see below for details) and a customized mount was used to align the objective with the GRIN lens. A pulsed NIR laser beam (λ = 920 nm; pulse width, 140 fs; repetition rate, 80 MHz) was generated by a Chameleon Ultra II (Coherent Corp., Santa Clara, CA) and it was modulated by a Pockels cell (Conoptics Inc., Danbury, CT).

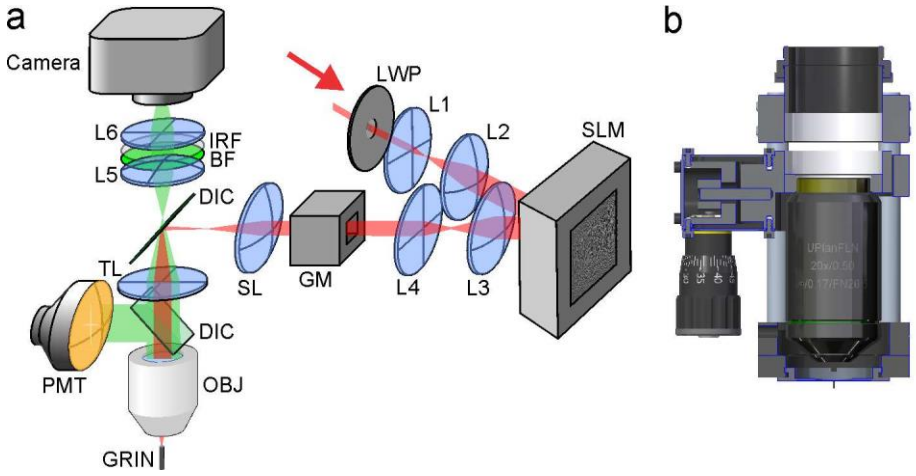

Fig. 1. a) Schematic of the optical system. LWP, half-lambda waveplate; L1-L2, beam expander lenses; SLM, phase only spatial light modulator; L3-L4, relay lenses; GM, galvo-mirror system; SL, scan lens; TL, tube lens; OBJ, microscope objective; GRIN, GRIN rod or GRIN microobjective; DIC, dichroic mirror; PMT, photomultiplier tube; L5-L6, image relay lenses; BF, barrier filter; IRF, near-infrared low-pass filter; camera, camera detector. b) Customized GRIN mounting system composed of a z translational mount (SM1Z, Thorlabs, Newton, NJ) which held the microscope objective. Proper positioning of the GRIN lens in the objective focal plane was obtained using a positioner (SPT1, Thorlabs, Newton, NJ).

A half-lambda waveplate (B.Halle Nachfl. GmbH, Berlin, GE) was used to reorient the beam polarization and to get pure phase modulation at the SLM (X10468-07 Hamamatsu Photonics, Hamamatsu, JP). A telescope (L1, f = 30 mm and L2, f = 75 mm; lens doublets IR coated, Thorlabs, Newton, NJ) was utilized to expand the beam to fill the SLM active window. Downstream the SLM, the beam was deflected onto the galvo-mirrors (GM) using a telescope (L3, f = 300 mm and L4, f = 150 mm; lens doublets IR coated, Thorlabs, Newton, NJ). The beam was then relayed to the back-aperture of the objective by the scan and tube lenses and finally focused by the microscope objective onto the back image plane of the GRIN lens. We employed two commercially available GRIN-based endomicroscopic lenses:

Biomedical Optics EXPRESS

i) a GRIN rod lens (NEM-050-25-10-860-S, Grintech GmbH, Jena, GE), with in-air external numerical aperture (NA) of 0.5 at the back side; ii) and a GRIN lens-based microobjective (GT-MO-080-018-810, Grintech GmbH, Jena, GE), with in-air external numerical aperture (NA) of 0.18 at the back side. The objectives coupling the GRIN lens to the microscope were: RMS20X-PF 20x, 0.5 NA (Olympus, Tokyo, JP) or LUCPlanFLN 60x, 0.7 NA (Olympus, Tokyo, JP) for the GRIN rod and UPlanFLN 10x 0.3 NA (Olympus, Tokyo, JP) for the GRIN microobjective. At the sample side, the maximal NA was 0.5 for the GRIN rod and 0.8 for the GRIN microobjective [21]. Both probes were designed to be immersed into water at the sample side with a working distance of 250 µm and 200 µm (for the GRIN rod and for the GRIN microobjective, respectively). Physical dimensions of the GRIN rod and GRIN microobjective (respectively) were: length, 1.86 mm and 7.5 mm; diameter, 0.5 mm and 1.4 mm. Two optical pathways were used for fluorescence collection. The first was based on photomultiplier- (PMT) mediated detection (Hamamatsu, Tokyo, JP). In the second, a telescope composed by L5 and L6 (f = 50 mm and f = 45 mm, respectively; doublets with VIS coating, Thorlabs, Newton, NJ) was used to relay the imaging plane onto the camera sensor (Orca-R2, Hamamatsu Photonics, Tokyo, JP or SciMeasure NeuroCCD-SMQ, Redshirt Imaging, Decatur, GA). The camera detection path also comprised a barrier filter (BF, ET525/50m, Chroma Technology Corp., Bellows Falls, VT) to reduce the visible autofluorescence photons, and a low-pass NIR filter (IRF, E750SP-2p8, Chroma Technology Corp., Bellow Falls, VT) to reduce back-reflected excitation photons. Custom software developed in LabView (National Instruments Corp., Austin, TX) was used to manage the phase retrieval algorithms and to interface the phase modulation with the laser scanning system. In most experiments, the optical pathway was designed so that the modulated component (first-order) of the laser beam was projected in a plane located ~30 - 50 µm above the unmodulated beam (zero-order). This was obtained illuminating the SLM with a slightly divergent beam and applying a proper defocus phase profile at the SLM. Under these conditions we obtained the collimated first-order component at the desired plane of interest and the divergent zero-order component projected on a deeper focal plane. Alternatively in a minority of experiments when a non-fluorescent region (e.g., the lumen of a blood vessel) was present at the center of the FOV, both the modulated and unmodulated components were kept in the same plane.

3. Results

To characterize the optical performances of our system, we first measured the point spread function (PSF) by imaging the fluorescence generated by sub-resolution fluorescent beads (Fig. 2(a), FluoSpheres; emission, 505 nm / 515 nm; diameter, 170 nm, Invitrogen Corp, Eugene, OR) in the two-photon scanning configuration using the PMT as detector and the projection of a single point. Full-width-half-maximum (FWHM; λ_{exc} = 920 nm) values of bead dimension showed nearly diffraction-limited resolution, given the degree of laser beam expansion at the objective backaperture on our set-up which had a standard configuration ($FWHM_{xy}$ = 0.81 ± 0.04 µm, $FWHM_z$ = 8.55 ± 0.35 µm, N = 10 for the GRIN rod. Figure 2(b); $FWHM_{xy}$ = 0.66 ± 0.08 µm, $FWHM_z$ = 3.21 ± 0.16 µm, N = 17 for the GRIN microbjective, Fig. 2(c)). These values were in good agreement with theoretical predictions [22,23] and with what reported elsewhere for other GRIN-based systems without the SLM unit [20]. We defined the maximum achievable holographic FOV as the maximal distance at which the fluorescence intensity of an illuminated point positioned using phase modulation through the SLM reaches 40% of the fluorescence intensity of an equal spot positioned in the center of the FOV (similarly to [24]). Values of the maximum achievable holographic FOV in the radial direction were: lateral, ~50 µm for the GRIN microobjective and ~140 µm for the GRIN rod. To interpret these values it is important to consider that in the optical configuration used in this experiment the GRIN microobjective had an effective magnification of 48x (4.8x microobjective, 10x coupling objective), whereas the GRIN rod

Biomedical Optics EXPRESS

displayed an effective magnification of 20x (1x rod, 20x coupling objective). The GRIN rod had thus a FOV that is 2.5 times larger than that of the GRIN microobjective. Moreover, the GRIN microobjective shows a steeper dependence of the NA with the radial distance [21] which may contribute to the smaller values of FOV observed with the GRIN microobjective. In the axial direction, we did not observe a decrease in the intensity below 40% for upward movements (from the microendoscope focal plane to the microendoscope frontend), while for downward movements the intensity dropped below 40% at ~40 µm for the GRIN microobjective and at ~140 µm for the GRIN rod.

We next measured the intensity profile along the z-axis of our excitation beam during simultaneous illumination with arrays of diffraction-limited points (Fig. 2(d)) which may be different from the $FWHM_z$ of the PSF that we measured above using the projection of a single diffraction-limited spot. To this aim we used sub-resolution fluorescent plastic layers [25].

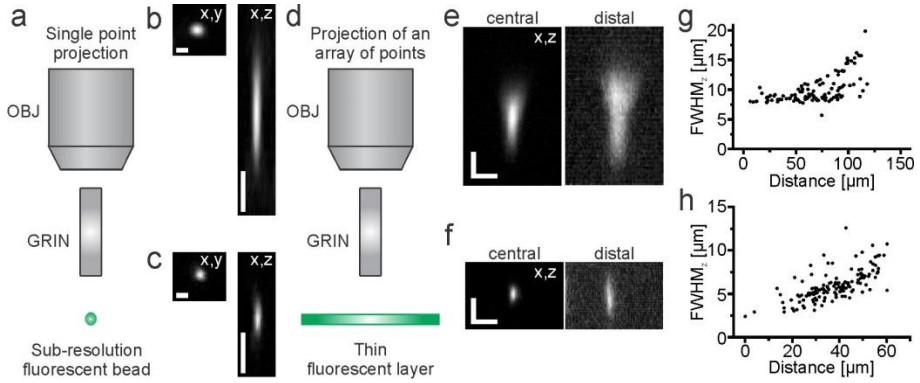

Fig. 2. a) Schematic of the experimental configuration. Subresolved fluorescent beads and a single excitation point, which was scanned using the galvanometric mirrors, were used for the measurement of the PSF. b-c) Images of a sub-resolution fluorescent bead in the x, y (left) and x, z (right) plane using the scanning system and the PMT as fluorescence detector for the GRIN rod (b) and the GRIN microobjective (c). Scale bars in b-c: 1 µm in the x,y projection (left image); 5 µm, in the x,z projection (right image). d) Schematic of the experimental configuration. A thin fluorescent layer was used as sample and an array of 17 diffraction-limited spots was projected on the sample. The camera was used as fluorescence detector. e-f) Fluorescence images showing the intensity profiles of a thin fluorescent layer along the z-axis for a spot in the central (left) and distal (right) part of the FOV during simultaneous projection of multiple spots using the GRIN rod (e) and the GRIN microobjective (f). Scale bars: 5 µm. g-h) $FWHM_z$ values as a function of the radial displacement for recordings performed in the optical configuration displayed in e-f for the GRIN rod (g) and the GRIN microobjective (h).

We generated a randomly distributed array of diffraction-limited spots (number of points in the array: 17) which were distributed evenly across the FOV with the SLM and acquired z-stacks using the camera as fluorescence detector. The intensity profiles along z-axis of one spot in the central (along the optical axis) and distal parts of the FOV are shown in Fig. 2(e), 2(f) for the GRIN rod and GRIN microobjective, respectively. The $FWHM_z$ values increased with the distance from the optical axis (Fig. 2(g), 2(h)), a result in agreement with the radial dependence of the NA in these microendoscopes [21].

Using a thick (1.4 mm) fluorescent plastic slide, we also characterized the uniformity of illumination, *u*, across different spots of the array (Fig. 3(a)) or across an extended shape (Fig. 3(b)-3(c)), with *u* defined as:

$$u = 1 - \frac{\sigma_I}{\bar{I}} \quad (1)$$

where σ_I is the standard deviation of the fluorescence intensity *I*, and $\bar{I}$ is the fluorescence intensity mean value across the points of an array or across an extended shape. The Weighted

Biomedical Optics EXPRESS

Gerchberg-Saxton (WGS) algorithm [26] was used to generate the phase modulation that was needed for the projection of the array of points.

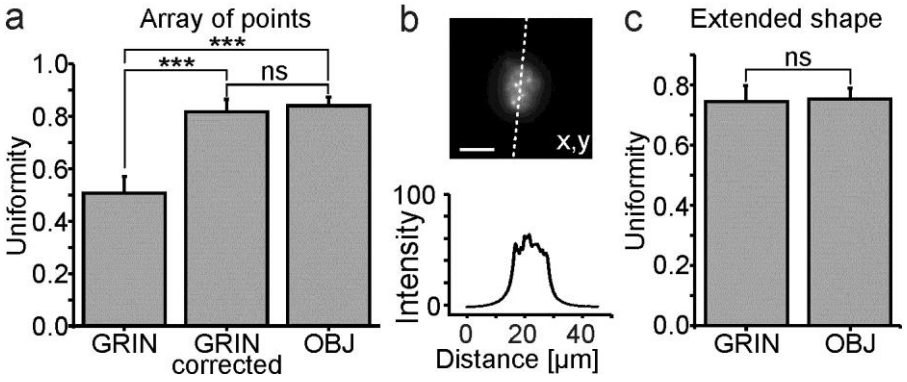

Fig. 3. a) Fluorescence uniformity for the projection of an array of points onto a thick fluorescent slide under the different experimental conditions. ***, $p < 0.001$; ns, non-significant, $p > 0.05$, one-way ANOVA, Bonferroni post hoc test ($N = 11$).The GRIN microobjective was used for experiments displayed in this figure. b) Top: fluorescence image acquired with a camera of a two-photon extended shape projected onto a thick fluorescent slide. Scale bar: 10 µm. Bottom: intensity profile along the direction indicated by the white dashed line in the top panel. c) Fluorescence uniformity for extended shapes illumination under the different experimental conditions. $p > 0.05$, paired Student's t-test ($N = 10$).

To investigate potential non-uniformities introduced by the GRIN lens, we compared the uniformity of an arrays of diffraction-limited points projected through the GRIN microobjective in the optical configuration shown in Fig. 1, with the uniformity of the same pattern of points projected through the microscope objective (Olympus 10x UPlanFLN, 0.3 NA) alone. For this measurement, the excitation points were generated within about 25 µm from the optical axis. Uniformity among the same pattern of points was significantly lower when the pattern was projected through the GRIN microobjective ($N = 11$, GRIN in Fig. 3(a)) compared to the objective alone (OBJ in Fig. 3(a)). To compensate for this effect, at the beginning of each imaging session we first created a phase map corresponding to an array of N points. We measured the fluorescence generated at every site (I_m, with $1 \le m \le N$) and calculated the average fluorescence across sites ($\bar{I}$) . If $\Delta I_m = |I_m - \bar{I}| / \bar{I} > 20\%$, we corrected the weight (w_m) used to superimpose the hologram corresponding to the m^{th}-site with the holograms of the other sites [26] with the scale factor ξ_m, defined as:

$$\xi_m \approx \left(\bar{I} / I_m \right)^{\rho} \tag{2}$$

where ρ is a parameter that tunes the strength of the correction and that varied in the interval [0.5,2], while ξ_m was constrained in the range [0.5,4]. We then generated a new phase map with w_m redefined as:

$$w_m^k \rightarrow \xi_m w_m^k \tag{3}$$

where ξ_m is fixed across the k algorithm iterations (with $k \in \mathbb{N}$). If $\Delta I_m > 20\%$ for more than one illumination site, the correction procedure was performed simultaneously for all those sites for which ΔI_m was > 20%. The correction procedure was iterated until the desired uniformity across sites was achieved. Using this strategy, we rescued the uniformity level of the objective alone (GRIN corrected in Fig. 3(a)).

We also tested the ability of our patterned illumination system to produce extended shapes (Fig. 3(b)) which were generated using the Gerchberg-Saxton algorithm [27]. For a shape 10 µm in diameter, the average axial resolution was 22 ± 2 µm (mean ± standard deviation; N =

Biomedical Optics EXPRESS

10). We compared the uniformity of extended shapes projected through the GRIN microobjective (in the optical configuration shown in Fig. 1) with the uniformity of the same extended shapes projected through the microscope 10x objective alone. No significant difference was observed between uniformity values under the two experimental configurations (Fig. 3(c)), suggesting that intensity variations due to speckles within the shape [12] could mask potential intensity non-homogeneities introduced by the GRIN microobjective itself.

We next applied our system to project complex patterns of two-photon excitation light onto fluorescent neuronal cells. We used patterned illumination with both arrays of points (Fig. 4(a)-4(d)) and extended shapes (Fig. 4(e)-4(h)) to test the potential applicability of our system to different experimental applications such as scanless functional imaging using arrays of points [4,5,28] or two-photon optogenetic manipulation through extended shapes [14,15]. For this experiment we used a slice of fixed neural tissue (slice thickness: 80 μm) in which neurons expressed the genetically encoded calcium indicator GCaMP6s [29]. GCaMP6s expression was obtained injecting mice at postnatal day 35 with an adenoassociated virus carrying the GCaMP6s construct under the hSynapsin promoter (AAV1.Syn.GCaMP6s.WPRE.SV40, UPenn Virus Core, PA). The fixed tissue was positioned on a rigid support that ensured mechanical stability. The sample was then imaged with the GRIN microobjective immersed in artificial cerebrospinal fluid solution (no glass coverslip on top of the brain slice) without inserting the GRIN probe in the tissue. An image was taken in scanning configuration with no phase modulation imposed to the SLM (Fig. 4(a), 4(e)) at a depth between 30 and 60 μm within the sample. This image was used to determine the target regions of interest to be illuminated with complex light patterns either a series of six diffraction-limited points (Fig. 4(b)) or two extended shapes (Fig. 4(f)) and compute the appropriate phase mask (Fig. 4(c), 4(g)) to be applied to the SLM. Patterned illumination was then applied to the sample, resulting in fluorescence excitation only in the desired locations (six points, Fig. 4(d) or two extended areas, Fig. 4(h)). Collection of excited fluorescence was performed with the camera.

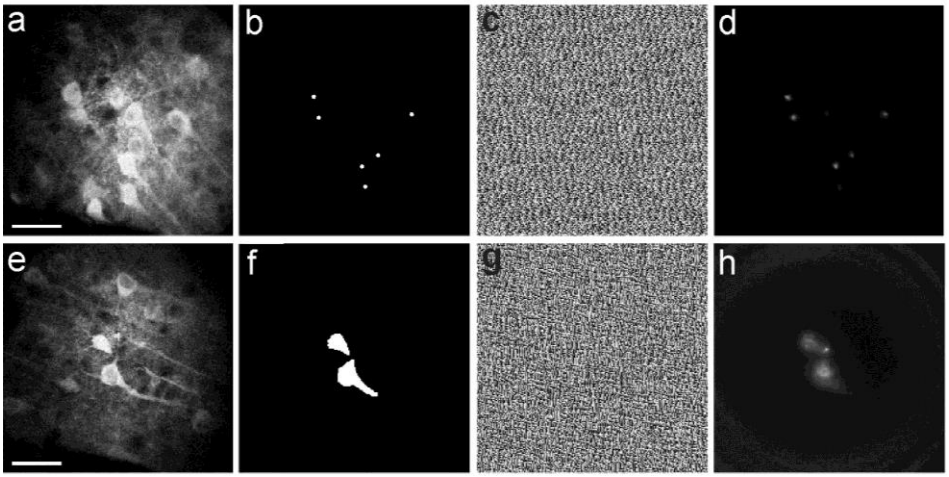

Fig. 4. a-d) Two-photon scanning image of a group of neurons expressing the Green Fluorescent Protein- (GFP) based calcium indicator GCaMP6s (a). The desired pattern of illumination (six diffraction-limited points, b) was identified based on the location of the cells observed in a. The corresponding phase mask (c) was generated and imposed to the SLM. The fluorescence image acquired with the camera and obtained applying the phase mask displayed in c is shown in d. Scale bar: 40 μm. e-h) Same as in a-d for a different field of view and illumination with two extended shapes. Scale bar: 40 μm.

Biomedical Optics EXPRESS

We finally applied our system to image functional signals from deep brain regions in the scanless configuration in anesthetized mice (C57BL/6J, Charles River, Calco, Italy) *in vivo*. Under isoflurane anesthesia, adult mice were injected with ~0.5 µl of a solution containing a combination of two viruses (AAV1.Syn.flex.GCaMP6s.WPRE.SV40 and AAV1.CaMKII0.4.Cre.SV40; ratio 1:1). Injection was performed using a glass pipette at stereotaxic coordinates corresponding to the hippocampal CA1 area (~50 nL/min; stereotaxic coordinates: 1.4 mm posterior to bregma, 1 mm lateral to the sagittal sinus and 1 mm deep [30];). After injection a small craniotomy (~600 x 600 μm^2) was performed over the neocortex at stereotaxic coordinates 1.8 mm posterior to bregma and 1.5 mm lateral to the sagittal sinus and a thin column of tissue was suctioned with a glass cannula with thin walls (cannula outside diameter: 700 µm; Vitrotubs, Vitrocom Inc. Mountain Lakes, NJ). The cannula was glued onto a plastic transparent support and moved in the three directions using a mechanical manipulator (Stoelting, Wood Dale, IL) guided by stereotaxic coordinates. After tissue removal, the GRIN rod was mounted on the same mechanical manipulator used to move the cannula and the GRIN rod was inserted in the hole created by tissue aspiration up to ~0.9 - 1 mm depth [30]. Given the working distance (250 µm) of the GRIN rod used, this experimental protocol resulted in imaging at ~1.2 mm depth within the mouse brain. Imaging depth was confirmed *a posteriori* by observing the endoscope track in the fixated brain tissue. Because the viral injection was performed just before endoscope insertion, it was not possible to image GCaMP fluorescence during endoscope placement and it was thus not feasible to choose a particular FOV during the insertion procedure. Once at the desired depth, the GRIN rod was secured by acrylic adhesive and dental cement to the skull, following standard procedures [20]. Under these experimental conditions the GRIN rod could not be moved in the axial direction, as instead was done in [31]. After surgery mice were recovered under a heating lamp and then returned to normal housing conditions in the animal facility. Three to four weeks after surgery mice were anesthetized with urethane, positioned onto a stereotaxic apparatus and the GRIN rod attached to their skull was aligned with the objective of the patterned two-photon microscope. All animal procedures were carried out according to the guidelines of the European Communities Council Directive and of the National Council on Animal Care of the Italian Ministry of Health (protocol #1134/2015-PR).

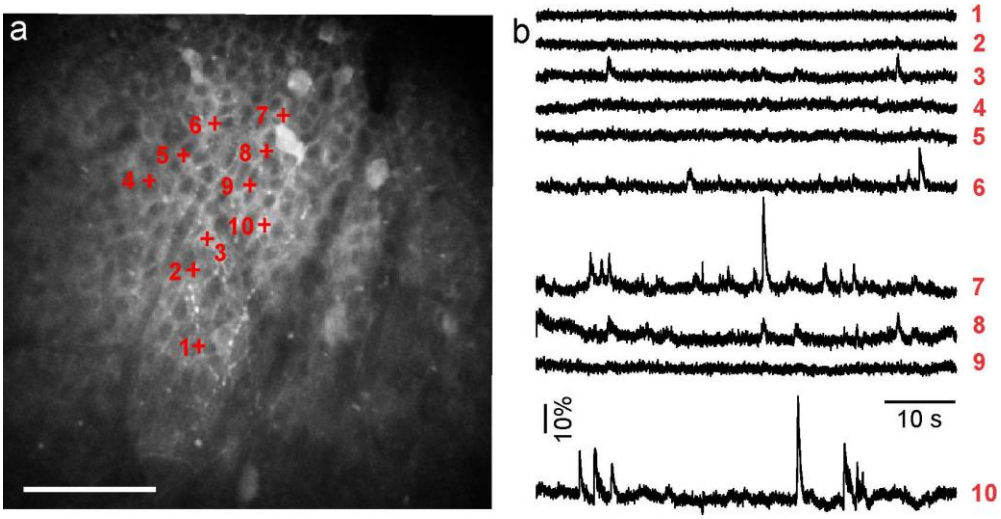

Fig. 5. a) Two-photon laser scanning image showing GCaMP6 expressing cells in the CA1 hyppocampus *in vivo*. Red crosses indicate the neurons that were imaged in the scanless configuration and that are numbered from 1 to 10. Scale bar: 100 µm. b) Fluorescence signals over time for the neurons displayed in the left panel recorded in scanless modality.

Biomedical Optics EXPRESS

We first took a high resolution image using galvanometric mirrors and the PMT to identify cells of interest in the hippocampal area (Fig. 5(a)) with no phase modulation imposed to the SLM. We then used the scanless imaging configuration [4,5,11] to deliver an array of diffraction-limited points (red crosses in Fig. 5(a); laser power: ~20 mW/point), with each point targeted to one cell. In this parallel excitation configuration fluorescence was collected over time with the camera (acquisition frequency: 40-125 Hz). Temporal series were then imported into the open soure ImageJ/Fiji software to identify the regions of interest (ROIs). The fluorescence signal of a given ROI was measured by computing the average intensity value in the four pixels located at the cented of the ROI. Fluorescence signals were analyzed with a custom software and the fluorescence changes were computed as $\Delta F/ F_0 = (F_t - F_0) / F_0$, where F_t is the fluorescence value at time *t*, and F_0 is the fluorescence baseline. Importantly, functional signals corresponding to activation of groups of hippocampal neurons could be clearly recorded under this experimental configuration (Fig. 5(b)).

4. Conclusions

In this study, we developed an optical system for patterned two-photon excitation through GRIN rods and GRIN microobjectives, and applied it for endomicroscopy applications in deep regions of the mouse brain. Complex light patterns could be projected at the sample plane, including arrays of points and extended shapes. Using thin fluorescent layers that allowed characterization of short working distance objectives as GRIN rods or GRIN-based microbjectives, we demonstrated that the z-extension of individual spots that were projected in arrays in the scanless configuration resembled the z-dimension of the PSF obtained with the two-photon laser scanning system and the projection of a single point. We showed that non-homogeneities in the excitation/detection pathways that resulted in variable efficiency in fluorescence excitation could be compensated by proper software control of the SLM. Moreover, we projected complex two-photon patterns of light onto fluorescent neurons, demonstrating that the system that we developed can be applied to the optical investigation of brain tissue. Finally, as direct proof of principle, we performed scanless functional imaging of hippocampal neural networks expressing the fluorescent calcium indicator GCaMP6 in anesthetized mice *in vivo*. Patterned illumination has been demonstrated in superficial cerebellar neurons using a fiberscope and single-photon stimulation [32]. Here, we show effective application of phase modulation in GRIN rods and GRIN microbjective using two-photon excitation for scanless functional imaging in deep (~1.2 mm) brain areas *in vivo*. An advantage of the two-photon scanless imaging configuration is the simultaneous excitation and detection of fluorescence in multiple regions of interest. If a fast fluorescence detector is used (e.g., a fast camera), high-speed (up to hundreds of Hz) mapping of multiple functional signals can be achieved in the scanless approach. This optical design might prove particularly important to investigate correlations (e.g., pairwise correlation or network correlation) among specific regions of interest within a given FOV. A limitation of scanless functional imaging is the crosstalk between the signals simultaneously emitted by adjacent regions of interest. This is especially relevant when imaging in highly scattering tissue as the mammalian brain. However, it is important to note that in our proof of principle experiment in the mouse hippocampus *in vivo* we used a GRIN rod with a working distance of 250 μm and we simultaneously recorded the fluorescence signal of ten different locations that were placed > 25 μm apart with no evident sign of crosstalk (Fig. 5).

These results will be fundamental to extend the potential of patterned two-photon illumination [11] for the functional investigation of subcortical structures and, more in general, all deep brain areas that can be accessed with a GRIN-based endomicroscopic probe.

Funding

Istituto Italiano di Tecnologia “Interdisciplinary - Interdepartmental project” to CL and TF and grants from European Research Council (ERC, NEURO-PATTERNS), FP7-Health

Biomedical Optics EXPRESS

(DESIRE), MIUR FIRB (RBAP11X42L), and NIH Brain Initiative (1U01NS090576-01) to TF.

Acknowledgments

We thank M. Dal Maschio for help in the initial stage of the study. V. Jayaraman, J. Akerboom, R. A. Kerr, D. S. Kim, L. L. Looger, K. Svoboda from the GENIE Project, Janelia Farm Research Campus, Howard Hughes Medical Institute for GCaMP constructs.